# Breakdown parameter for kinetic modeling of multiscale gas flows

# Breakdown parameter for kinetic modeling of multiscale gas flows

Jianping Meng,[1,*] Nishanth Dongari,[2,†] Jason M. Reese,[3,‡] and Yonghao Zhang[1,§]
[1]*James Weir Fluids Laboratory, Department of Mechanical and Aerospace Engineering, University of Strathclyde, Glasgow G1 1XJ, United Kingdom*
[2]*Department of Mechanical & Aerospace Engineering, Indian Institute of Technology Hyderabad, Ordnance Factory Estate Yeddumailaram 502205, India*
[3]*School of Engineering, University of Edinburgh, Edinburgh, EH9 3 JL, United Kingdom*
(Received 9 September 2013; published 13 June 2014)

Multiscale methods built purely on the kinetic theory of gases provide information about the molecular velocity distribution function. It is therefore both important and feasible to establish new breakdown parameters for assessing the appropriateness of a fluid description at the continuum level by utilizing kinetic information rather than macroscopic flow quantities alone. We propose a new kinetic criterion to indirectly assess the errors introduced by a continuum-level description of the gas flow. The analysis, which includes numerical demonstrations, focuses on the validity of the Navier-Stokes-Fourier equations and corresponding kinetic models and reveals that the new criterion can consistently indicate the validity of continuum-level modeling in both low-speed and high-speed flows at different Knudsen numbers.

DOI: 10.1103/PhysRevE.89.063305 PACS number(s): 47.11.−j, 47.45.−n, 47.61.−k

## I. INTRODUCTION

In microelectromechanical systems (MEMS) that depend on gas flows, there may be coexisting continuum-fluid and highly rarefied regions [1]. To qualitatively identify the rarefaction level of the local flowfield, the Knudsen number (Kn) is often used, which is the ratio of the mean free path of gas molecules to a characteristic length scale of the flow process. It is commonly accepted that the conventional hydrodynamic description is only valid for $\mathrm{Kn} < 0.001$. When Kn is larger than 0.001, rarefaction effects have to be taken into account. Rarefied flows can be further classified into the slip ($0.001 \leqslant \mathrm{Kn} \leqslant 0.1$), transitional ($0.1 \leqslant \mathrm{Kn} \leqslant 10$), and free molecular ($\mathrm{Kn} \geqslant 10$) flow regimes.

Multiscale methods are needed when gas flows have a broad range of rarefaction levels (see, for example, Refs. [2–15], and references therein). The conventional Navier-Stokes-Fourier (NSF) equations are computationally efficient but are only valid in the hydrodynamic regime. Although their capabilities may be extended into the slip flow regime by applying appropriate velocity-slip and temperature-jump boundary conditions, their applicability range is strictly limited. By contrast, accurate kinetic gas solvers, including the direct simulation Monte Carlo (DSMC) method [16] and direct solution of the Boltzmann equation [17], can be computationally very expensive. Therefore, to strike a balance between computational costs and simulation accuracy, multiscale schemes are being developed that take advantage of both kinetic and continuum-fluid solvers, i.e., deploying a kinetic solver only in the rarefied flow regions and a continuum solver in the hydrodynamic regions. The two types of method are coupled together by exchanging information at interfaces where they overlap.

However, it has not proven easy to exchange information between two methods with different theoretical frameworks. It is problematic for the continuum solver to recover the accurate information required by the kinetic method [12]. Although the kinetic model can provide the information necessary for the continuum model, it can be computationally expensive [4]. The statistical noise associated with particle methods may also affect the accuracy and stability of the hybrid solver [12].

Recently, several new multiscale schemes have been constructed purely on the basis of gas kinetic theory [18–21]; we call these kinetic multiscale schemes (KMS) here. A distinctive feature of KMS is that the same evolutional quantity (i.e., the molecular velocity distribution function) is used to describe flowfields with different rarefaction levels, leading to relatively easy information exchange at the model coupling interfaces [19,20]. To capture different levels of rarefaction, usually different discrete velocity sets are necessary. In general, more discrete velocities are needed for higher levels of rarefaction, and fewer discrete velocities are required for lower levels of rarefaction. In particular, there have been efforts to design schemes specialized in continuum-level modeling, e.g., the gas-kinetic Bhatnagar-Gross-Krook (BGK) Burnett solutions [22]. This provides a good opportunity to improve the efficiency of multiscale solvers. It is important practically to use fewer discrete velocities, or specialized continuum-level solvers, as widely as possible in the flow field wherever they are valid.

For example, only a small number of lattice velocities are required for the lattice Boltzmann model to achieve NSF-order accuracy, e.g., nine for two-dimensional isothermal simulations. However, 16 or more lattice velocities are needed in order to achieve Burnett-order accuracy. For even higher accuracy, more velocities are required. Hence, a typical multiscale lattice Boltzmann scheme [19] may employ 16 lattice velocities in the regions where the NSF equations are valid and even more lattice velocities for other more rarefied regions; e.g., see Fig. 10 in Ref. [19]. However, since the same governing equation is used over the whole flowfield,

*jianping.meng@strath.ac.uk
†nishanth@iith.ac.in
‡jason.reese@ed.ac.uk
§To whom the correspondence should be addressed: yonghao.zhang@strath.ac.uk

 

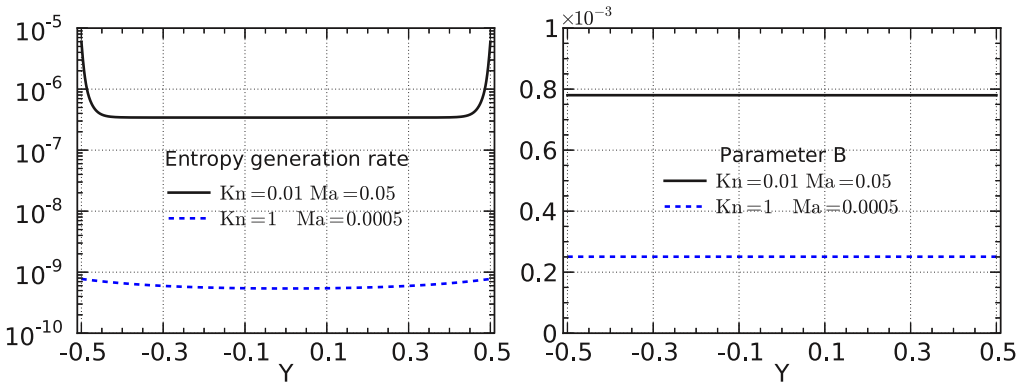


FIG. 1. (Color online) Cross-channel profiles of (left) the entropy generation rate [28] and (right) parameter B [26] for low-Mach-number planar Couette flows. The flows are solved with the linearized-BGK equation by using Gauss-Hermite quadrature. The Mach number is defined as $\mathrm{Ma} = U_w/\sqrt{RT_0}$ and the Knudsen number is $\mathrm{Kn} = \sqrt{\pi/2}[\mu_0\sqrt{RT_0}/(P_0 L)]$ (see Sec. III). The planar channel walls are at $[-0.5, 0.5]$.

information exchange between the region can be accomplished by using simple interpolation and extrapolation operations.

An appropriate equilibrium breakdown parameter plays a key role in the success of any multiscale scheme, such as KMS. In order to couple kinetic methods and continuum-fluid solvers together, a breakdown parameter is required to determine where and when to switch between the two types of model. As a continuum model is not valid for highly rarefied flows, it is necessary to assess the modeling error introduced whenever it is applied. For simulation efficiency, the continuum solver should be deployed in the flowfield as widely as possible as long as it satisfies the requirement for solution accuracy. For KMS, a continuum-fluid model breakdown parameter is still of key importance. If a computational region is known to be solvable by the NSF equations, optimized kinetic solvers can be used to achieve better efficiency as discussed above, e.g., the nine lattice velocity model.

Various breakdown parameters have been proposed in the literature. The global Knudsen number has often been used [2]. Other parameters are also suggested, such as Tsien's parameter [23], Bird's parameter $P$ [24], the local Knudsen number [13,14], Tiwari's criterion [25], the parameter $B$ [26], the criterion proposed by Lockerby *et al.* [2], and some others [27,28]. Although these breakdown parameters have had some success, in particular, for high-speed flows, it is fair to say that there is no general parameter available. It remains an open research question to identify a general continuum model breakdown parameter for quantifying modeling accuracy. In particular, most of the available parameters are based on macroscopic quantities, which does not take advantage of the kinetic level information available in KMS.

Our aim here is to devise new breakdown parameters for KMS. The central idea is to make best use of the kinetic level information in KMS provided by the molecular velocity distribution function (from which the relevant macroscopic quantities can also be obtained). The resulting parameters should not solely depend on macroscopic flow properties, unlike other available parameters.

## II. CONTINUUM MODEL BREAKDOWN

The development of previous continuum model breakdown parameters has been based on the Boltzmann equation and its asymptotic solution [29]. The Boltzmann equation describes the dynamical behavior of dilute gases, under the assumptions of binary collisions between gas molecules and of molecular chaos. A single molecular velocity distribution function describes the gas motion.

Various series solution methods have been used to tackle the Boltzmann equation. Among them, the Chapman-Enskog

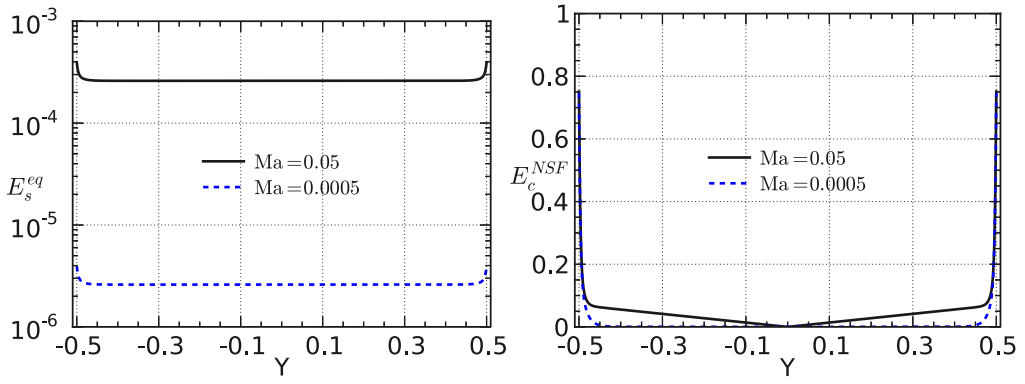


FIG. 2. (Color online) Cross-channel profiles of $E_s^{\mathrm{eq}}$ (left) and $E_c^{\mathrm{NSF}}$ (right) for linear Couette flows at $\mathrm{Kn} = 0.01$. The planar channel walls are at $[-0.5,0.5]$.

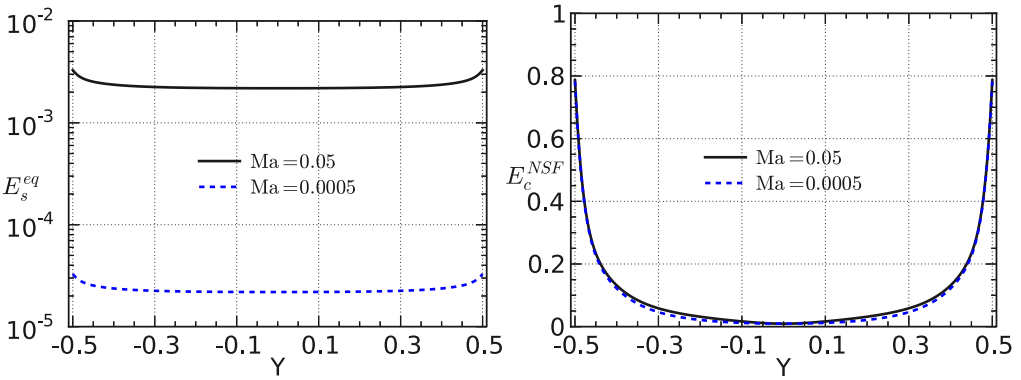


FIG. 3. (Color online) Cross-channel profiles of $E_s^{\mathrm{eq}}$ (left) and $E_c^{\mathrm{NSF}}$ (right) for linear Couette flows at Kn = 0.1. The planar channel walls are at [−0.5,0.5].

expansion [29] is widely used to approximate the distribution function as

$$f = f^{(0)} + f^{(1)} + f^{(2)} + \cdots + f^{(\alpha)} + \cdots, \tag{1}$$

where the distribution functions $f^{(\alpha)}$ in increasing orders in Kn can be obtained from the Boltzmann equation. The Maxwell-Boltzmann equilibrium distribution,

$$f^{\mathrm{eq}} = \frac{\rho}{(2\pi RT)^{3/2}} \exp\left[-\frac{\varsigma^2}{2RT}\right], \tag{2}$$

is the zeroth-order solution $f^{(0)}$ and leads to the Euler hydrodynamic equations. Here, $\rho$ denotes the gas density; $T$ the temperature; $R$ the gas constant; $\boldsymbol{\varsigma}$ the peculiar velocity of molecules (which is $\boldsymbol{\xi} - \boldsymbol{u}$, where $\boldsymbol{\xi}$ represents the molecular velocity); and $\boldsymbol{u}$ is the macroscopic fluid velocity.

In Eq. (1), $f^{(1)}$ provides a nonequilibrium correction of the order of the small parameter Kn. The NSF-level estimation for $f^{(1)}$ is

$$f^{(1)} \approx f^{\mathrm{NSF}} \approx f^{\mathrm{eq}}\left[\left(\frac{\sigma_{ij}\varsigma_{<i}\varsigma_{j>}}{2pRT}\right) + \frac{2q_i\varsigma_i}{5pRT}\left(\frac{\varsigma^2}{2RT} - \frac{5}{2}\right)\right], \tag{3}$$

where $p$ is the gas pressure, and the shear stress $\sigma_{ij}$ and the heat flux $q_i$ are related to the following first-order gradients of velocity and temperature:

$$\sigma_{ij} = -2\mu\frac{\partial u_{<i}}{\partial x_{j>}}, \quad q_i = -\kappa\frac{\partial T}{\partial x_i}, \tag{4}$$

where $\mu$ and $\kappa$ denote the viscosity and thermal conductivity. Here we only keep the first-order Sonine expansion term, which is exact for Mawellian gases (see, e.g., Refs. [29,30] for detail); however, this is expected to be sufficient for our purpose. In fact, at the core of KMS is often an appropriate kinetic model equation (e.g., the BGK model) rather than the Boltzmann equation, which provides information of NSF-level accuracy at the first order of the Sonine expansion.

Following the same principle, we can obtain $\alpha$-order (with respect to small Kn) corrections to the equilibrium distribution function. So higher-order hydrodynamic equations can be derived, e.g., the Burnett and super Burnett equations. As an alternative to the Chapman-Enskog expansion, the moment method provides a different way of solving the Boltzmann equation and leads to a number of extended hydrodynamic models, e.g., Grad-13 [31], R13 [32], R26 [33]. Therefore, regarding a continuum-fluid model breakdown parameter, we need to keep in mind which set of hydrodynamic equations or what order kinetic model are used [34].

As the NSF equations or NSF-level kinetic models are used by most multiscale methods we will focus on this continuum model. Also, since the applicability of the continuum fluid model has been effectively extended well beyond the NSF

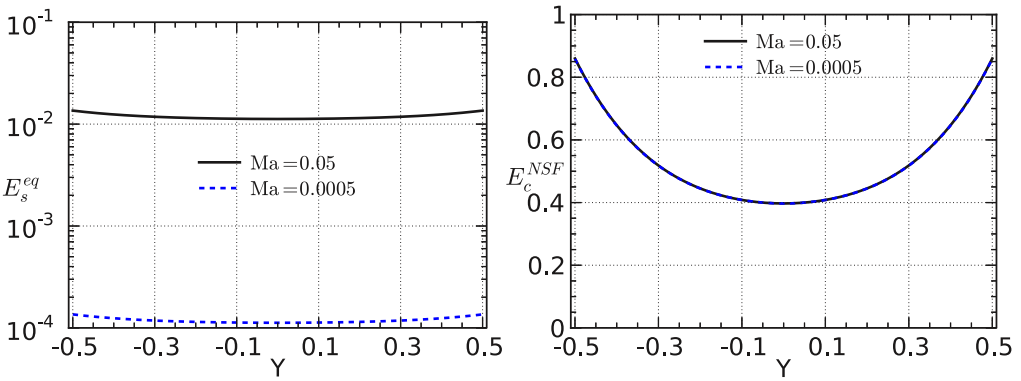


FIG. 4. (Color online) Cross-channel profiles of $E_s^{\mathrm{eq}}$ (left) and $E_c^{\mathrm{NSF}}$ (right) for linear Couette flows at Kn = 1. The planar channel walls are at [−0.5,0.5].

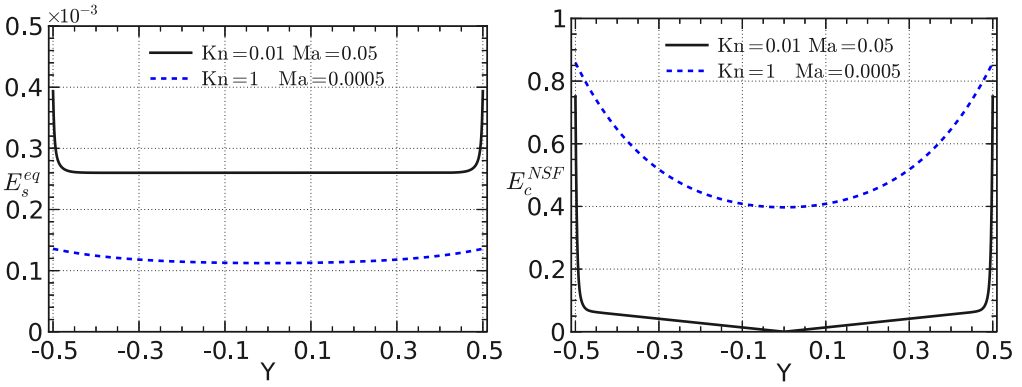


FIG. 5. (Color online) Cross-channel comparison of $E_s^{\rm eq}$ (left) and $E_c^{\rm NSF}$ (right) for linear Couette flows at Kn = 0.01 and Kn = 1 for small Mach numbers. The planar channel walls are at [−0.5,0.5].

equations [30], hereafter, "continuum breakdown" refers to the failure of the NSF equations, or the NSF-order kinetic model.

To establish a continuum breakdown parameter, and taking our lead from the Chapman-Enskog expansion, we separate the distribution function into three parts, i.e., $f^{\rm eq}$, $f^{\rm NSF}$, and $f^H$ as

$$f = f^{\rm eq} + f^{\rm NSF} + f^H, \tag{5}$$

where $f^H$ represents all higher-order nonequilibrium corrections. From the Chapman-Enskog expansion, we can use $f^{\rm NSF}$ from Eq. (3) to recover the NSF model. The higher-order corrections $f^H$ produce the Burnett equations and beyond.

Therefore, we may directly use the information provided by $f^{\rm eq}$, $f^{\rm NSF}$, and $f^H$ to assess the validity of the NSF equations and an NSF-order kinetic model. For assessing other high-order models, such as the Burnett equations and the R13 model, $f^H$ needs to be split further.

The Chapman-Enskog expansion indicates that there are various levels of nonequilibrium corrections to the equilibrium distribution function. As "nonequilibrium" is a very broadly used term, in this paper we equate the level of nonequilibrium to how far the molecular velocity distribution function deviates from the local Maxwellian equilibrium distribution. So the Euler equations are the continuum model for describing locally equilibrium flows, and the NSF equations provide a first-order nonequilibrium correction. A comparison of $f - f^{\rm eq}$ to $f^{\rm eq}$ indicates the deviation from equilibrium, and hence indirectly assesses whether the Euler equations are a valid model or not. When we examine the validity of the NSF equations and an NSF-order kinetic model, we may indirectly evaluate $f^{\rm NSF}$ and $f^H$, then for the NSF equations to be sufficiently accurate, $f^{\rm NSF}$ should be significantly larger than $f^H$ so that the high-order corrections can be neglected. Many previous breakdown parameters were based on comparing nonequilibrium corrections with the equilibrium component, which is more appropriate for examining the validity of the Euler equations than the NSF equations.

Let us consider simple linear cases, where the leading order of $f^{\rm eq}$ is $\mathcal{O}(1)$, while that of $f^{\rm NSF}$ can be represented by the shear stress term $\sim\mu\partial u_{<i}/\partial x_{j>}$, which is $\mathcal{O}$(MaKn), cf. Eq. (3). Therefore, as a breakdown parameter, using either $f^{\rm NSF}$ itself or a ratio $\sim f^{\rm NSF}/f^{\rm eq}$ will lead to be the order $\mathcal{O}$(MaKn). Here Ma is the Mach number, which is defined as the ratio of characteristic speed to the sound speed (see, e.g., Sec. III for the definition for Couette flows). However, for a linear flow condition the Mach number is not relevant to the validity of the NSF equations. This can be confirmed through numerical simulations of simple Couette flow, as shown in Fig. 1, where two parameters are evaluated, namely, the entropy generation rate from Ref. [28] and the parameter B from Ref. [26]. For kinetic model equations, the entropy generation rate can be calculated as $\frac{1}{\tau}\int(f^{\rm eq} - f)\log f d\boldsymbol{\xi}$, where $\tau$ is the relaxation time. The parameter B depends on macroscopic quantities, i.e., $B = \max(|\sigma_{ij}|,|q_i|)$. As can be seen in Fig. 1 both parameters fail to perform well as

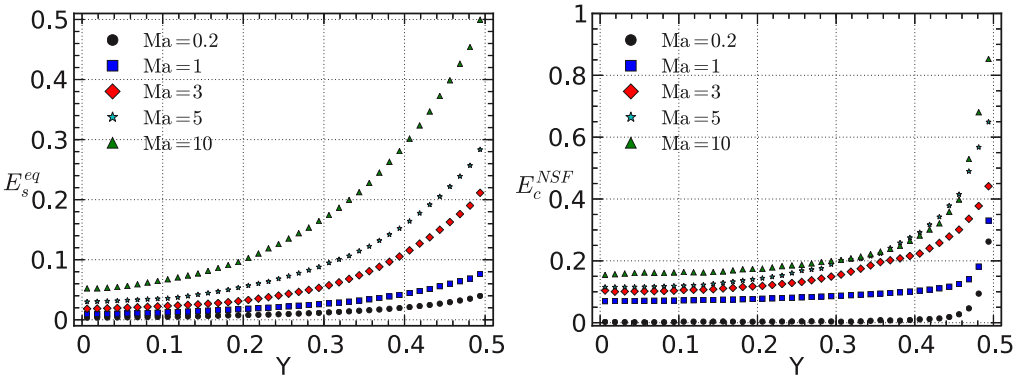


FIG. 6. (Color online) Half-channel profiles of $E_s^{\rm eq}$ and $E_c^{\rm NSF}$ for nonlinear Couette flows at Kn = 0.01.

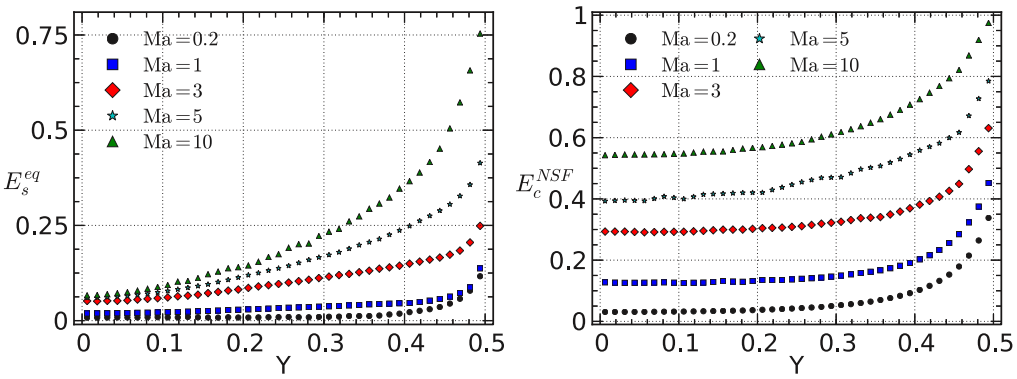


FIG. 7. (Color online) Half-channel profiles of $E_s^{\mathrm{eq}}$ and $E_c^{\mathrm{NSF}}$ for nonlinear Couette flows at Kn = 0.1.

breakdown parameters for the NSF equations: both the entropy generation rate and parameter B are significantly smaller for larger Knudsen number (Kn = 1.0), where the NSF equations are not valid, than for smaller Knudsen number (Kn = 0.01), where the NSF equations may be applicable with velocity-slip and temperature-jump boundary conditions.

It is also interesting to estimate the order of the ratio of $f^{\mathrm{NSF}}$ to $f^H$. For this purpose, $f^H$ may be approximated by the Burnett level solution when the Chapman-Enksog expansion is valid (one may refer to Ref. [35] for a relatively simpler form of the Burnett equations). With this approximation, we find that the leading order of $f^H$ is $\mathcal{O}(\mathrm{MaKn}^2)$ under the linear flow condition. It immediately follows that the ratio of $f^{\mathrm{NSF}}$ to $f^H$ is of the order of Kn, which is a reasonable indication of the validity of the NSF equations under the linear flow condition. For a strong nonlinear flow condition with Ma $>$ 1, we find that the leading order of $f^H$ would be $\mathcal{O}(\mathrm{Ma}^2\mathrm{Kn}^2)$ due to the occurrence of squared gradient terms. Then the ratio of $f^{\mathrm{NSF}}$ to $f^H$ may lead to a quantity $\sim$MaKn. This provides a reasonable indication of the validity of the NSF equations under nonlinear conditions as there have been successes in applying such parameters' proportional to MaKn (e.g., Tsien's and Bird's parameters) for strong nonlinear cases. These observations indicate the feasibility of using $f^{\mathrm{NSF}}$ and $f^H$ to evaluate the validity of the NSF equations or of NSF-order kinetic models.

Equation (5) can also be understood outside the Chapman-Enskog expansion. We can simply split the distribution function $f$ into three parts, i.e., $f^{\mathrm{eq}}$, $f^{\mathrm{NSF}}$, and $f^H$, which are not subject to the small Knudsen number assumption of the Chapman-Enskog expansion. For an NSF solution to be valid, any additional non-equilibrium corrections should be small in comparison to $f^{\mathrm{NSF}}$. If $f^H$ is comparable to $f^{\mathrm{NSF}}$ or even larger, the NSF equations or an NSF-order kinetic model are not sufficient. A similar approach has been used in Ref. [2] to obtain breakdown parameters based on macroscopic flow properties. We call this approach here the "NSF breakdown indicator," and it could provide a better way of assessing the NSF equations indirectly.

Based on the above discussion, our proposed NSF breakdown indicator $E_c^{\mathrm{NSF}}$ is

$$E_c^{\mathrm{NSF}} = \sqrt{\frac{\int (f^{(H)})^2 d\boldsymbol{\xi}}{\int (f^{\mathrm{NSF}})^2 d\boldsymbol{\xi}}} = \sqrt{\frac{\int (f - f^{\mathrm{eq}} - f^{\mathrm{NSF}})^2 d\boldsymbol{\xi}}{\int (f^{\mathrm{NSF}})^2 d\boldsymbol{\xi}}}. \tag{6}$$

In the following sections we numerically examine whether $E_c^{\mathrm{NSF}}$ is an appropriate breakdown indicator for an NSF solution. We also give numerical evidence to show that the measurement of deviation from equilibrium may not work, although many other breakdown parameters use similar ideas (e.g., the B parameter and the entropy generation rate shown in Fig. 1). At the kinetic level, this latter deviation (we call it the "nonequilibrium indicator") is measured by

$$E_s^{\mathrm{eq}} = \sqrt{\frac{\int (f - f^{\mathrm{eq}})^2 d\boldsymbol{\xi}}{\int (f^{\mathrm{eq}})^2 d\boldsymbol{\xi}}} = \frac{\sqrt{8}\pi^{3/4}(RT)^{3/4}}{\rho} \sqrt{\int (f - f^{\mathrm{eq}})^2 d\boldsymbol{\xi}}. \tag{7}$$

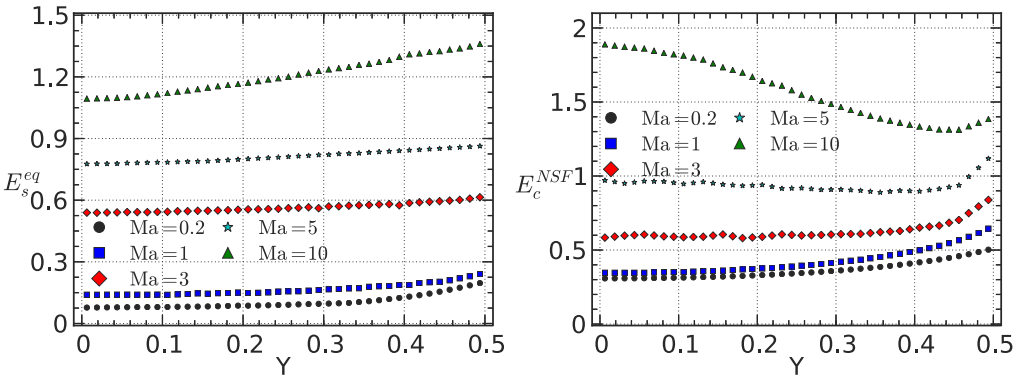


FIG. 8. (Color online) Half-channel profiles of $E_s^{\mathrm{eq}}$ and $E_c^{\mathrm{NSF}}$ for nonlinear Couette flows at Kn = 1.

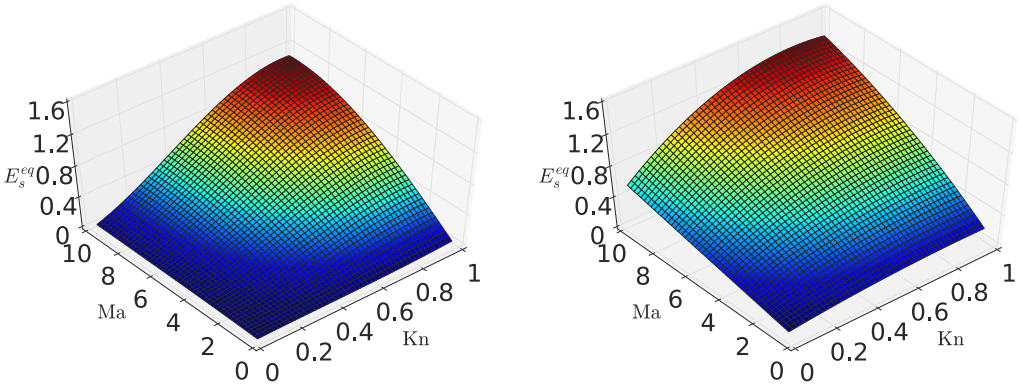


FIG. 9. (Color online) Dependence of $E_s^{\mathrm{eq}}$ on Kn and Ma in the bulk (left) and at the wall (right).

We use the $L^2$ norm to assess $E_c^{\mathrm{NSF}}$ and $E_s^{\mathrm{eq}}$. In our framework, $E_s^{\mathrm{eq}}$ assesses the nonequilibrium level and $E_c^{\mathrm{NSF}}$ estimates the appropriateness of an NSF solution. As both these parameters are based purely on the molecular distribution function, we term them "kinetic breakdown parameters."

In fact, both Eq. (6) and Eq. (7) are standard formulations for measurement of relative errors. Therefore, $E_c^{\mathrm{NSF}}$ and $E_s^{\mathrm{eq}}$ are estimating the solution error relative to the correction $f^{\mathrm{NSF}}$ and the equilibrium function $f^{\mathrm{eq}}$, respectively. It can be easily seen that a larger $E_c^{\mathrm{NSF}}$ means larger errors in the solution. Due to this direct connection, a "cutoff" value of $E_c^{\mathrm{NSF}}$, i.e., where a model switch should be conducted, may be determined from practical considerations. For example, a 10% error may be chosen as this value, as in the Couette flow cases discussed below.

## III. NUMERICAL INVESTIGATION

To examine $E_s^{\mathrm{eq}}$ and $E_c^{\mathrm{NSF}}$ we first use shear-driven planar Couette flow as a benchmark. Here, the two bounding surfaces are moving with speeds $U_w$ in opposite directions, and their temperatures are set to $T_0$. The Mach number is $\mathrm{Ma} = U_w/\sqrt{RT_0}$, and the Knudsen number is $\mathrm{Kn} = \sqrt{\pi/2}[\mu_0\sqrt{RT_0}/(P_0L)]$, where $L$ is the flow channel width and $P_0$ is the reference pressure. The NSF equations should be applicable for small Knudsen numbers, but will fail to predict the nonlinear Knudsen layers at the walls. Many proposed breakdown parameters are not appropriate for this type of flow, as already indicated from Fig. 1. This therefore serves as a good benchmark case to evaluate different breakdown parameters.

We first investigate linear (low-speed) Couette flows. The simulations are accomplished by solving the linearized BGK equation with the discrete velocity method [36]. It is worth noting that all the quanities in this work are nondimensionalized using the system reported in Ref. [36] (see page 385). In Figs. 2, 3, and 4 it is clearly seen that $E_s^{\mathrm{eq}}$ is negligibly small for low-speed Couette flows, even at relatively large Knudsen numbers (e.g., $\mathrm{Kn} = 1$). This indicates that the flows can be close to equilibrium at large Knudsen number, although the NSF equations will still fail. Therefore, alongside many other parameters, including the entropy generation rate and the parameter B, $E_s^{\mathrm{eq}}$ is not an appropriate breakdown parameter for the NSF equations or an NSF-order kinetic model. In Fig. 5, $E_s^{\mathrm{eq}}$ and $E_c^{\mathrm{NSF}}$ are explicitly plotted for two different Knudsen numbers: $E_s^{\mathrm{eq}}$ is smaller in the case of larger Knudsen number ($\mathrm{Kn} = 1$), while $E_c^{\mathrm{NSF}}$ increases for increasing Knudsen numbers.

For nonlinear Couette flows (i.e., when $\mathrm{Ma} \geqslant 0.2$), we perform molecular dynamics (MD) simulations using the OpenFOAM code that includes the MD routines implemented by Reese and coworkers [37–39]. Monatomic Lennard-Jones argon molecules are simulated [40], and initially the molecules are spatially distributed in the Couette flow domain with a random Gaussian velocity distribution corresponding to an initially prescribed gas temperature. They are then allowed to relax through collisions until reaching a steady state before we take measurements. This MD solver has been previously validated for both liquids and gases confined in arbitrary geometries. To achieve measurement of a smooth velocity distribution function at steady state, molecular velocity samples are taken in every time step ($0.001\tau$, where $\tau = \sqrt{md^2/\epsilon}$, with $m$ being the molecular mass, $d$ the diameter of gas molecules, and $\epsilon$ being related to the interaction strength of the molecules) for a total time of at least 30 000$\tau$ (in the extreme rarefied and high speed flow case below, up to 100 000$\tau$). We have 83 500 molecules in each simulation, and apply diffuse wall interactions.

The measurement sampling is performed in the microcanonical ensemble consisting of a constant number of atoms, constant volume, and constant energy. Each case is solved in parallel on 16 cores of the 1100 core high performance compute facility at the University of Strathclyde. The equations of molecular motion are integrated using a leapfrog scheme with the simulation time step of 5 fs. The actual run time for each case ranges from 50 to 200 h, depending on the level of rarefaction, for which we were able to simulate 1000 ns of problem time after reaching the steady state. The simulation domain is divided into 80 bins in the wall-normal direction to measure macroscopic field properties, such as temperature. In each bin, there are approximately 1000 molecules in order to measure local macroscopic properties, and averaging occurs over 30–100 million time samples in the steady-state regime so as to minimize numerical errors.

The resulting profiles of $E_s^{\mathrm{eq}}$ and $E_c^{\mathrm{NSF}}$ for various nonlinear Couette flow cases are presented in Figs. 6, 7, and 8. In these flows nonequilibrium and rarefaction effects are coupled: $E_s^{\mathrm{eq}}$ shows the level of nonequilibrium in the local flowfield, while $E_c^{\mathrm{NSF}}$ indicates the inapplicability of the NSF equations (or an NSF-order kinetic model) with increasing Mach number and

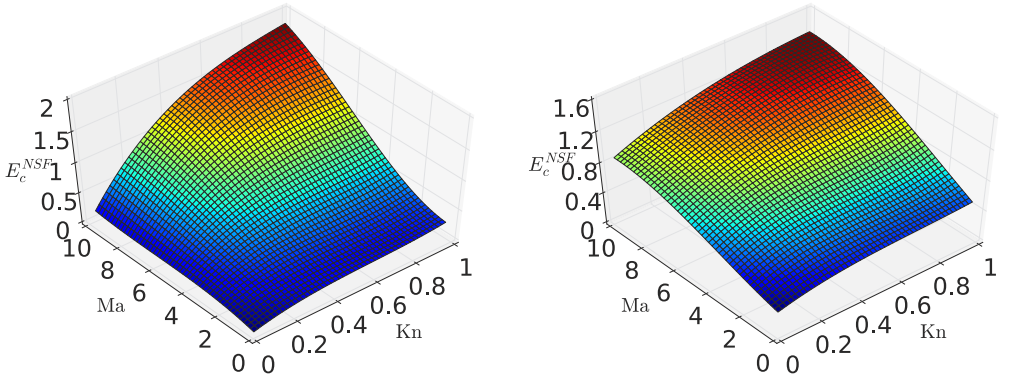


FIG. 10. (Color online) Dependence of $E_c^{\mathrm{NSF}}$ on Kn and Ma in the bulk (left) and at the wall (right).

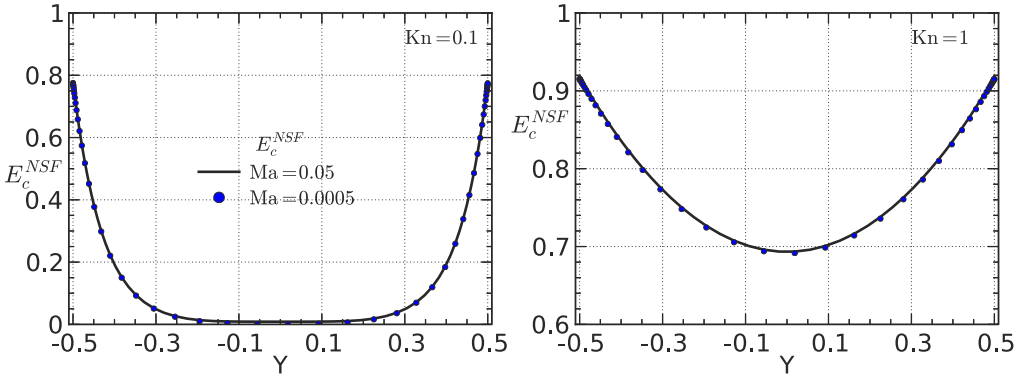


FIG. 11. (Color online) Cross-channel profiles of $E_c^{\mathrm{NSF}}$ predicted by a 16-velocity lattice model for linear Couette flows at Kn = 0.1 and 1. The planar channel walls are at [−0.5,0.5].

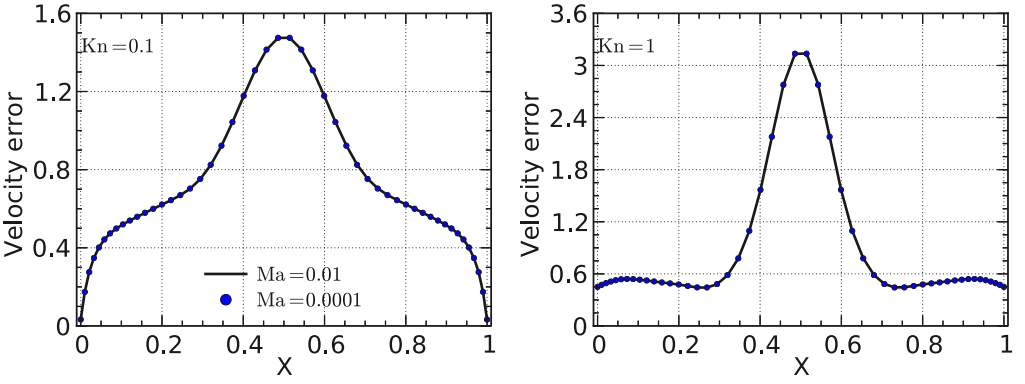


FIG. 12. (Color online) Lid-driven cavity flow; profiles of errors of the velocity field along the horizontal line $Y = 0.627$.

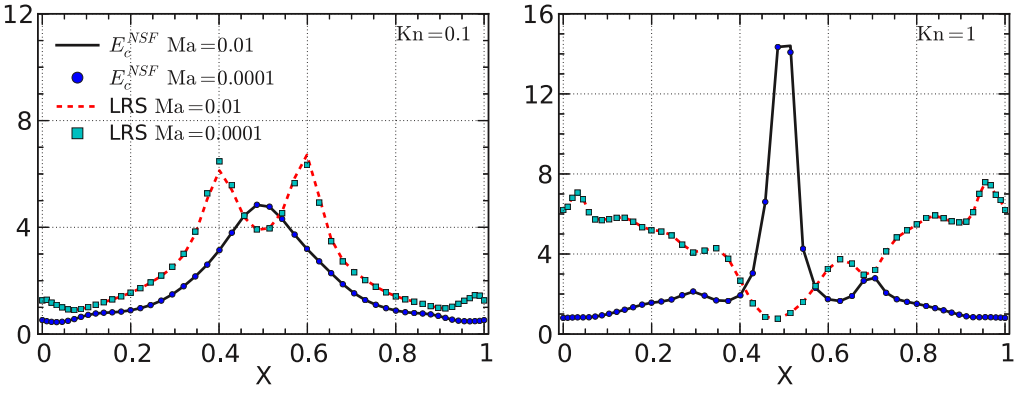


FIG. 13. (Color online) Lid-driven cavity flow; profiles of $E_c^{\mathrm{NSF}}$ predicted from the 400-velocity model and the parameter LRS along the horizontal line $Y = 0.627$.

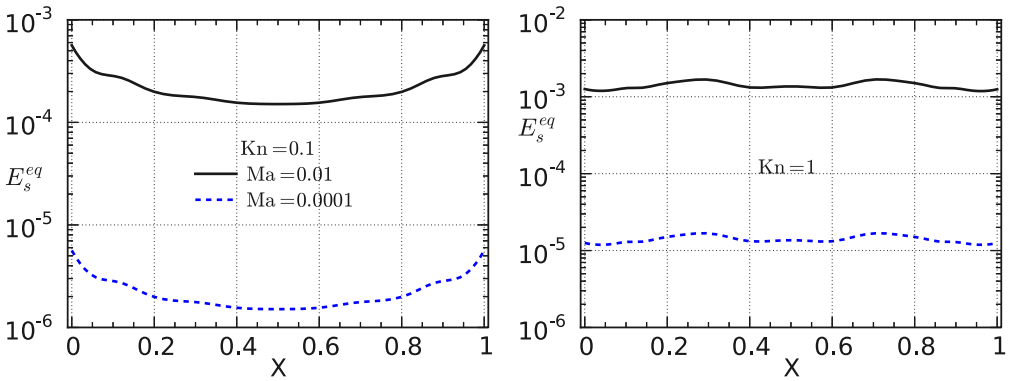


FIG. 14. (Color online) Lid-driven cavity flow; profiles of $E_s^{\mathrm{eq}}$ predicted from the 400-velocity lattice model along the horizontal line $Y = 0.627$.

Knudsen number. In contrast to the linear (low-Mach number) Couette flow case, $E_s^{\mathrm{eq}}$ seems to be able to indicate the error induced by the NSF model. This may be the reason why some parameters that measure deviation from equilibrium, such as Tsien's parameter, the parameter B, and the entropy generation rate, have some success for high-speed flows. But only $E_c^{\mathrm{NSF}}$ works consistently, for both linear and nonlinear Couette flows, as a breakdown indicator for the NSF model or an NSF-order kinetic model.

To understand how the Knudsen and Mach numbers affect $E_s^{\mathrm{eq}}$ and $E_c^{\mathrm{NSF}}$, we present their dependencies on Kn and Ma in Figs. 9 and 10. These clearly indicate the complicated coupled effects of rarefaction and nonequilibrium varying with the Knudsen number and the Mach number. When the Mach number is small, the flow is close to equilibrium regardless of the Knudsen number. For a small $E_c^{\mathrm{NSF}}$, the Knudsen number must be small; but $E_c^{\mathrm{NSF}}$ can also be significant when the Knudsen number is still small (see Fig. 10). This indicates that an NSF solution may be invalid even with relatively small Knudsen numbers.

In the above cases, the parameters were evaluated using numerical solutions at molecular resolution. While $E_c^{\mathrm{NSF}}$ appears to be able to give reasonable indications, we wish to investigate now whether this parameter can use results from a less accurate model in order to assess whether it needs to switch to a more accurate model. In Ref. [19], we demonstrated how to couple two lattice Boltzmann models (e.g., with 16 and 36 lattice velocities for 2D simulations) at prescribed interfaces where the lower-order model is employed on 70% of the computational region in the center of the channel. In Fig. 11, the results of the 16-velocity model are presented for linear Couette flows at Kn = 0.1 and Kn = 1. We see that $E_c^{\mathrm{NSF}}$ calculated from this low-order model can reasonably indicate where the lower-order model needs to be switched to a higher-order model. For the case of Kn = 0.1, $E_c^{\mathrm{NSF}}$ predicts errors of about 10% at $y = \pm 0.35$, which indicates that it is better to switch models at these points. For the case of Kn = 1, $E_c^{\mathrm{NSF}}$ suggests that the higher-order model should be used exclusively, as the error is always larger than 60%. In both cases the predictions of $E_c^{\mathrm{NSF}}$ are consistent with the practice in Ref. [19].

To further test $E_c^{\mathrm{NSF}}$, we simulate a lid-driven cavity flow. In this flow, the gas is contained in a two-dimensional rectangular geometry with four walls. Both the length in the $x$ direction and the height in the $y$ direction are set to be $L$, which is therefore considered as the reference length to define the Knudsen number. The top wall is moving from left to right while the other three walls are stationary. The lid speed is set to be 0.01 and 0.0001 for various cases and is used to define the characteristic Mach number, i.e., the ratio of the lid speed and $\sqrt{RT_0}$ where $T_0$ is the wall temperature. The simulations are performed using lattice Boltzmann models for Kn = 0.1 and Kn = 1: NSF-level solutions are provided by the 9-velocity lattice Boltzmann model, while a 400-velocity model serves to provide the benchmark results. In these simulations, we compare with the error in the predicted velocity field, which is calculated as $\sqrt{(u_C - u_E)^2 + (v_C - v_E)^2}/\sqrt{u_C^2 + v_C^2}$, where

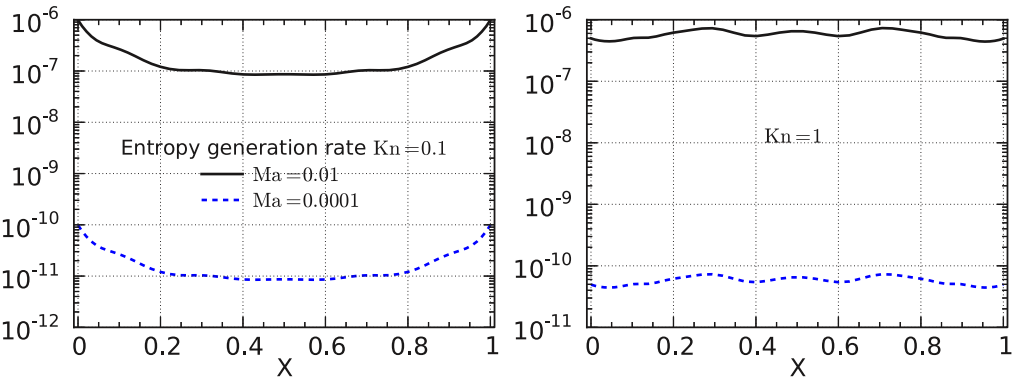


FIG. 15. (Color online) Lid-driven cavity flow; profiles of the entropy generation rate along the horizontal line $Y = 0.627$.

the subscript $C$ represents the "correct" solution provided by the 400-velocity lattice Boltzmann model, and subscript $E$ represents the results from the 9-velocity lattice model; $u$ and $v$ denote the horizontal and vertical velocity components, respectively.

As shown in Figs. 12–15, $E_c^{\mathrm{NSF}}$ calculated from the 400-velocity lattice model gives consistent predictions that qualitatively match the distribution of error in the velocity field in Fig. 12. In Fig. 13 the parameter proposed by Lockerby *et al.* [2] (LRS for short) is also plotted for comparison. While both $E_c^{\mathrm{NSF}}$ and the LRS parameter are based on the same fundamental idea, the better prediction of $E_c^{\mathrm{NSF}}$ for this flow may be attributed to the fact that the distribution functions contain more information than the macroscopic flow quantities used in LRS.

## IV. CONCLUDING REMARKS

On the fundamental basis of the molecular velocity distribution function, we have discussed how to evaluate the appropriateness of a locally applied continuum level kinetic solver for a gas flow. A breakdown parameter $E_c^{\mathrm{NSF}}$ has been proposed for NSF-order kinetic solvers so that we can apply the most efficient kinetic solver in flow regions where the NSF-level description is sufficient. For instance, in these regions a smaller number of discrete velocities may be used to reduce the computational burden if the kinetic multiscale scheme uses the discrete velocity method, the multiscale lattice Boltzmann model [19], or the unified gas kinetic scheme [18]. The application of the criterion can be fairly straightforward: both $f^{\mathrm{eq}}$ and $f^{\mathrm{NSF}}$ can be calculated using Eq. (2) and Eq. (3), respectively. As most kinetic solvers use the distribution function $f$ and require the evaluation of $f^{\mathrm{eq}}$, the calculation of $E_c^{\mathrm{NSF}}$ in kinetic multiscale schemes introduces only a small additional computational cost.

By using Couette flows and lid-driven cavity flows as test cases, we have demonstrated the encouraging capability of $E_c^{\mathrm{NSF}}$ as a breakdown parameter. However, investigations of further flow problems are necessary in order to assess issues such as the cutoff value where a model switch should be conducted. Although $E_c^{\mathrm{NSF}}$ itself is mathematically a $L^2$ norm form of error estimation, and so provides intuitive guidance, the determination of the cutoff value may be problem-dependent and needs to be calibrated by studying more flows.


[1] G. Karniadakis, A. Beskok, and N. Aluru, 1st ed., *Microflows and Nanoflows: Fundamentals and Simulation (Interdisciplinary Applied Mathematics)* (Springer, Berlin, 2005).
[2] D. A. Lockerby, J. M. Reese, and H. Struchtrup, Proc. R. Soc. A **465**, 1581 (2009).
[3] S. Tiwari, A. Klar, and S. Hardt, J. Comput. Phys. **228**, 7109 (2009).
[4] Q. Sun, I. D. Boyd, and G. V. Candler, J. Comput. Phys. **194**, 256 (2004).
[5] T. E. Schwartzentruber and I. D. Boyd, J. Comput. Phys. **215**, 402 (2006).
[6] T. E. Schwartzentruber, L. C. Scalabrin, and I. D. Boyd, J. Comput. Phys. **225**, 1159 (2007).
[7] H. S. Wijesinghe and N. G. Hadjiconstantinou, Int. J. Mult. Comput. Eng. **2**, 189 (2004).
[8] P. L. Tallec and F. Mallinger, J. Comput. Phys. **136**, 51 (1997).
[9] J.-F. Bourgat, P. L. Tallec, and M. D. Tidriri, J. Comput. Phys. **127**, 227 (1996).
[10] S. T. O'Connell and P. A. Thompson, Phys. Rev. E **52**, R5792 (1995).
[11] J. M. Burt and I. D. Boyd, J. Comput. Phys. **228**, 460 (2009).
[12] N. G. Hadjiconstantinou, Bull. Pol. Ac.: Tech **53**, 335 (2005).
[13] I. D. Boyd, G. Chen, and G. V. Candler, Phys. Fluids **7**, 210 (1995).
[14] W.-L. Wang and I. D. Boyd, Phys. Fluids **15**, 91 (2003).
[15] D. A. Kessler, E. S. Oran, and C. R. Kaplan, J. Fluid Mech. **661**, 262 (2010).
[16] G. A. Bird, Annu. Rev. Fluid Mech. **10**, 11 (1978).
[17] S. M. Yen, Annu. Rev. Fluid Mech. **16**, 67 (1984).
[18] K. Xu and J.-C. Huang, J. Comput. Phys. **229**, 7747 (2010).
[19] J. Meng, Y. Zhang, and X. Shan, Phys. Rev. E **83**, 046701 (2011).
[20] V. V. Aristov, A. A. Frolova, S. A. Zabelok, V. I. Kolobov, and R. R. Arslanbekov, *Computational Fluid Dynamics 2006* (Springer, Berlin, 2009), pp. 719–724.
[21] V. I. Kolobov, R. R. Arslanbekov, V. V. Aristov, A. A. Frolova, and S. A. Zabelok, J. Comput. Phys. **223**, 589 (2007).
[22] K. Xu and Z. Li, J. Fluid Mech. **513**, 87 (2004).
[23] H. S. Tsien, J. Aerospace Sci. **13**, 342 (1946).
[24] G. A. Bird, AIAA J. **8**, 1998 (1970).
[25] S. Tiwari, J. Comput. Phys. **144**, 710 (1998).
[26] A. L. Garcia and B. J. Alder, J. Comput. Phys. **140**, 66 (1998).
[27] M. N. Macrossan, in *Twenty-Fifth International Symposium on Rarefied Gas Dynamics, St. Petersburg, Russia*, edited by M. S. Ivanov and A. K. Rebrov (Siberian Branch of the Russian Academy of Sciences, Russia, 2007), pp. 759–764.
[28] S. Chigullapalli, A. Venkattraman, M. S. Ivanov, and A. A. Alexeenko, J. Comput. Phys. **229**, 2139 (2010).
[29] S. Chapman and T. G. Cowling, 3rd ed., *The Mathematical Theory of Non-Uniform Gases* (Cambridge University Press, Cambridge, 1953).
[30] H. Struchtrup, *Macroscopic Transport Equations for Rarefied Gas Flows: Approximation Methods in Kinetic Theory (Interaction of Mechanics and Mathematics)* (Springer, Berlin, 2005).
[31] H. Grad, Commun. Pure Appl. Maths **2**, 331 (1949).
[32] H. Struchtrup and M. Torrilhon, Phys. Fluids **15**, 2668 (2003).
[33] X.-J. Gu and D. R. Emerson, J. Fluid Mech. **636**, 177 (2009).
[34] G. A. Radtke, Jean-Philippe, M. Praud, and N. G. Hadjiconstantinou, Philos. Trans. R. Soc. A **371**, 1471 (2013).
[35] Y. Zheng and H. Struchtrup, Continuum Mech. Thermodynam. **16**, 97 (2004).
[36] J. Meng, L. Wu, J. M. Reese, and Y. H. Zhang, J. Comput. Phys. **251**, 383 (2013).
[37] G. B. Macpherson, M. K. Borg, and J. M. Reese, Mol. Simul. **33**, 1199 (2007).
[38] G. B. Macpherson, and J. M. Reese, Mol. Simul. **34**, 97 (2008).
[39] M. K. Borg, G. B. Macpherson, and J. M. Reese, Mol. Simul. **36**, 745 (2010).
[40] N. Dongari, Y. Zhang, and J. M. Reese, J. Phys. D: Appl. Phys. **44**, 125502 (2011).